

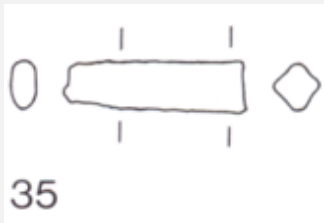
# TANG FRAGMENT OF A KNIFE HR-6246 – TIN BRONZE – LATE BRONZE AGE – SWITZERLAND

**Artefact name** Tang fragment of a knife HR-6246

**Authors** Marianne. Senn (Empa, Dübendorf, Zurich, Switzerland) & Christian. Degrigny (HE-Arc CR, Neuchâtel, Neuchâtel, Switzerland)

**Url** /artefacts/977/

## ∨ The object



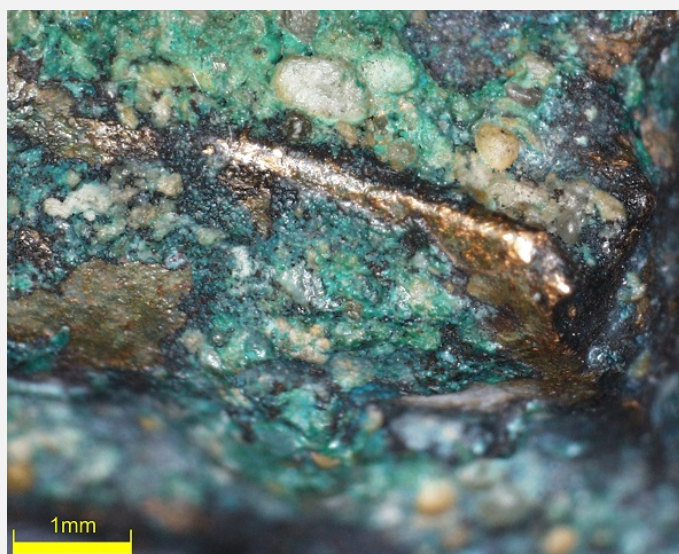
*Credit HE-Arc CR.*



*Credit HEI-Arc CR, N.Gutknecht.*

Fig. 1: Tang fragment of a knife (after Rychner-Faraggi 1983, plate 35.35),

Fig. 2: Lake (shiny brown) and terrestrial (granulated green-blue) crust covering the tang with lacuna on the right showing the underlying metal and detail of Fig. 3,



*Credit HE-Arc CR, N.Gutknecht.*

Fig. 3: Detail of Fig. 2 (rotated by 180°),

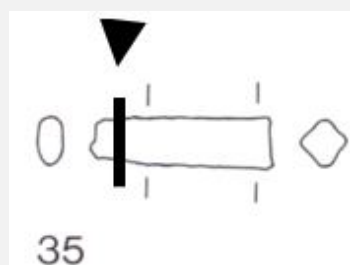
## ∨ Description and visual observation

<b>Description of the artefact</b>	Tang fragment of a knife with lake (shiny brown) and terrestrial (granulated green-blue) crust (Fig. 1). Dimensions: L = 2.7cm; Ø = around 5mm; WT = 5.8g.
<b>Type of artefact</b>	Knife
<b>Origin</b>	Hauterive - Champréveyres, Neuchâtel, Neuchâtel, Switzerland
<b>Recovering date</b>	Excavation 1983-1985, object from layer 1 (layer with material from Bronze Age till 20th cent.)
<b>Chronology category</b>	Late Bronze Age
<b>chronology tpq</b>	<input type="text" value="1050"/> B.C. ▾
<b>chronology taq</b>	<input type="text" value="800"/> B.C. ▾
<b>Chronology comment</b>	Hallstatt A/B
<b>Burial conditions / environment</b>	Lake
<b>Artefact location</b>	Laténium, Neuchâtel, Neuchâtel
<b>Owner</b>	Laténium, Neuchâtel, Neuchâtel
<b>Inv. number</b>	Hr 6246
<b>Recorded conservation data</b>	N/A

## Complementary information

Considered to be a land patina by Schweizer (1994).

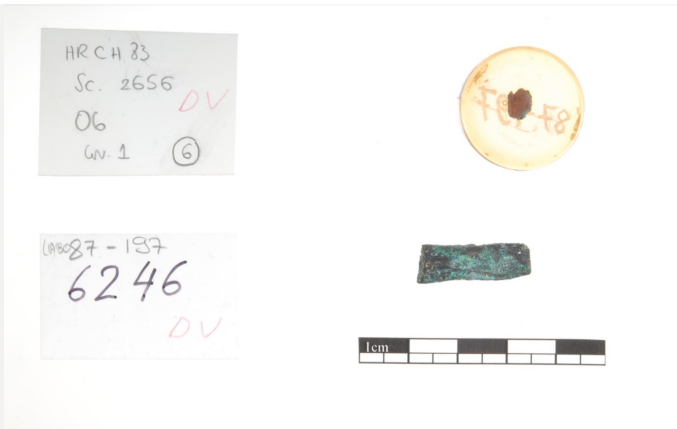
## ∨ Study area(s)



Credit HE-Arc CR.

Fig. 4: Location of sampling area,

Fig. 5: Cross-section of the tang and remaining material,



Credit Laténium, C.Cevey.

Binocular observation and representation of the corrosion structure

The schematic representation below gives an overview of the corrosion layers encountered on the tang from a first visual macroscopic observation.

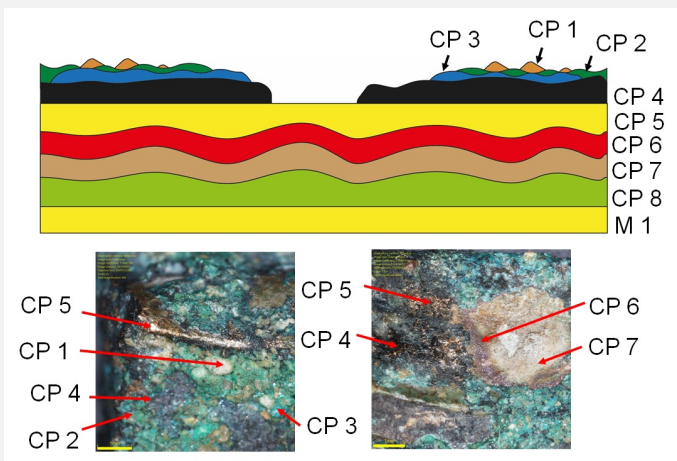


Fig. 6: Stratigraphic representation of the tang fragment and location of the strata,

Credit HE-Arc CR, N.Gutknecht.

MiCorr stratigraphy(ies) – Bi

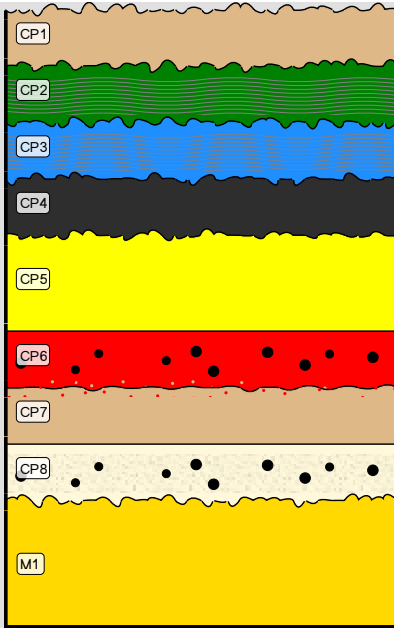


Fig. 7: Stratigraphic representation of the corrosion structure of the tang fragment observed macroscopically under binocular microscope using the MiCorr application. The characteristics of the strata are only accessible by clicking on the drawing that redirects you to the search tool by stratigraphy representation, Credit HE-Arc CR.

Sample(s)

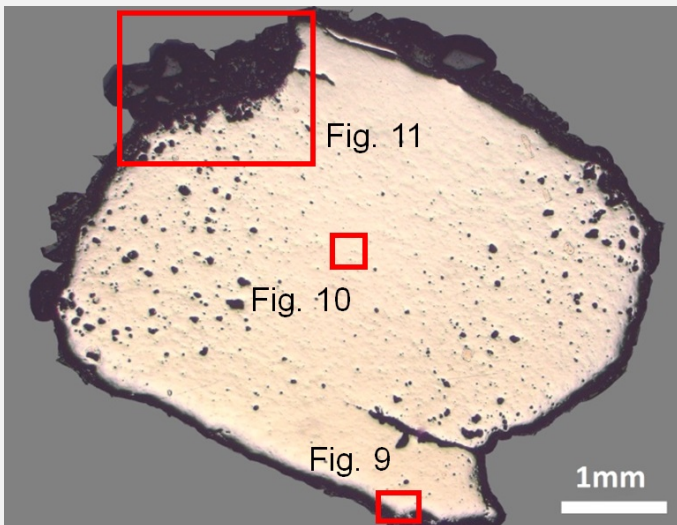


Fig. 8: Micrograph of the cross-section of the sample taken from the tang fragment showing the location of Figs. 9 to 11,

Credit HE-Arc CR.

<b>Description of sample</b>	The cross-section corresponds to a lateral cut (Fig. 4). The surface is covered with a thick corrosion crust but part of it has gone (Fig. 8).
<b>Alloy</b>	Tin Bronze
<b>Technology</b>	Cold worked after annealing
<b>Lab number of sample</b>	MAH 87-197
<b>Sample location</b>	Musées d'art et d'histoire, Genève, Geneva
<b>Responsible institution</b>	Musées d'art et d'histoire, Genève, Geneva
<b>Date and aim of sampling</b>	1987, metallography and corrosion characterisation

## Complementary information

This sample is mentioned in Schweizer, 1994.

### ∨ Analyses and results

#### **Analyses performed:**

Metallography (etched with ferric chloride reagent), Vickers hardness testing, ICP-OES, SEM/EDS, XRD.

### ∨ Non invasive analysis

None.

### ∨ Metal

The remaining metal is a tin bronze (Table 1) with high porosity (Fig. 8) and large cracks both on the left and right edges of the sample (Fig. 8). The metal contains small, elongated copper sulphide (Table 2) and Pb inclusions that are oriented parallel to the cracks. Near the metal surface, slip lines are outlined by the development of intergranular corrosion (Fig. 9). The etched metal shows small, elongated grains. Slip lines are also visible (Fig. 10). Annealing is visible in areas near the surface. The average hardness of the metal is HV1 145, but significant variations are observed, depending on where the measurements are taken.

Elements	Cu	Sn	Sb	Ni	Pb	As	Ag	Co	Fe	Zn
mass%	89.85	8.02	0.60	0.55	0.34	0.34	0.18	0.10	0.02	0.01

Table 1: Chemical composition of the metal. Method of analysis: ICP-OES, Laboratory of Analytical Chemistry, Empa.

Elements	O	S	Cu	Total
mass%	0.9	20	77	98

Table 2: Chemical composition of inclusions. Method of analysis: SEM/EDS, Laboratory of Analytical Chemistry, Empa.

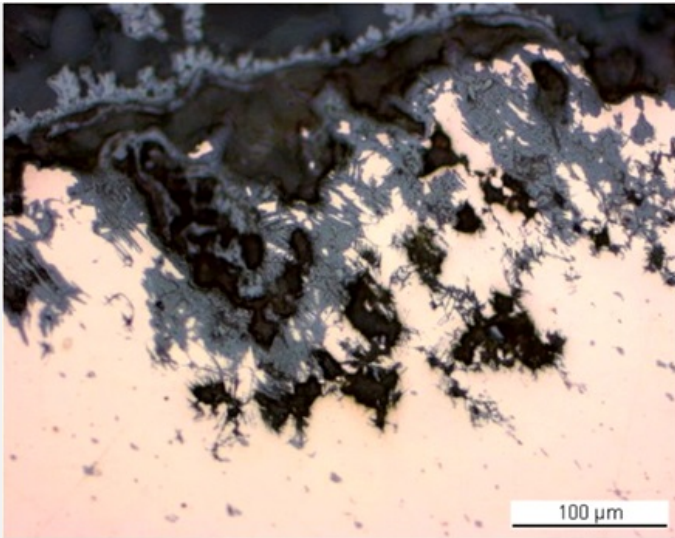


Fig. 9: Micrograph of the metal sample from Fig. 8 (inverted and reversed picture, detail), unetched, bright field. Corrosion products are in dark-grey whereas the metal is in pink. Slip lines are outlined by the development of intergranular corrosion,

Credit HE-Arc CR.

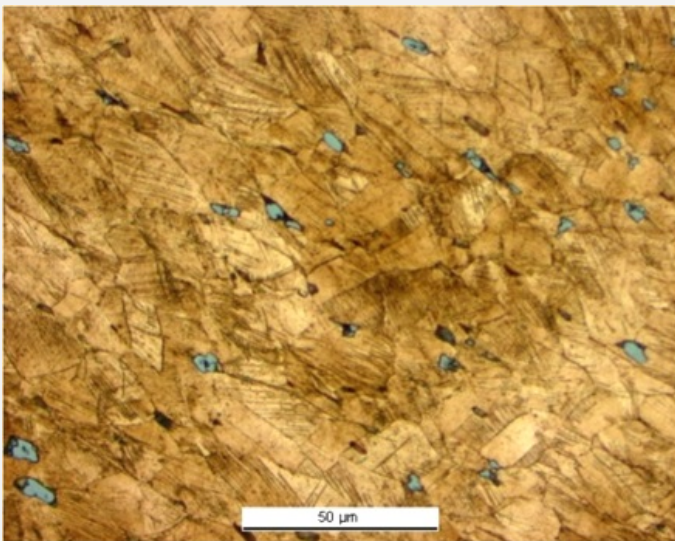


Fig. 10: Micrograph of the metal sample from Fig. 8 (detail), etched, bright field. We observe elongated grains with slip lines as well as grey copper sulphide inclusions,

Credit HE-Arc CR.

<b>Microstructure</b>	Elongated grains + strain lines with pores
<b>First metal element</b>	Cu
<b>Other metal elements</b>	Co, Ni, As, Ag, Sn, Sb, Pb

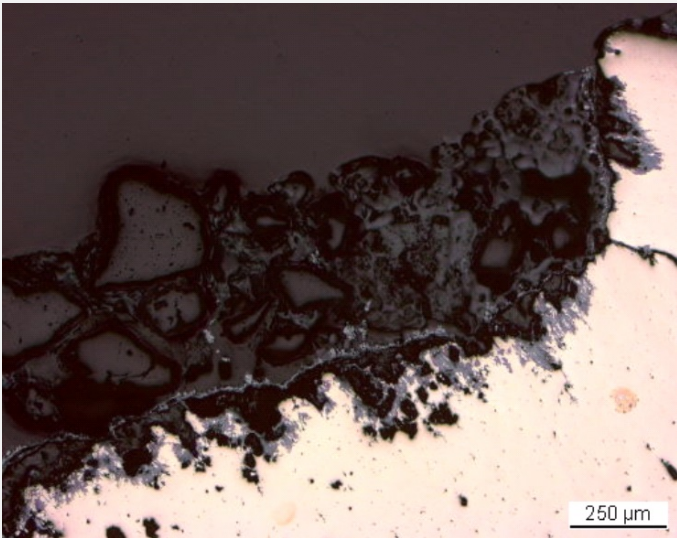
#### Complementary information

Schweizer (1994) indicates that the copper-tin alloys similar to the one of the tang have minor constituents that were certainly not added intentionally. Furthermore, he mentions that there is no systematic composition difference between bronzes with a lake patina and those with a land patina.

#### ✕ Corrosion layers

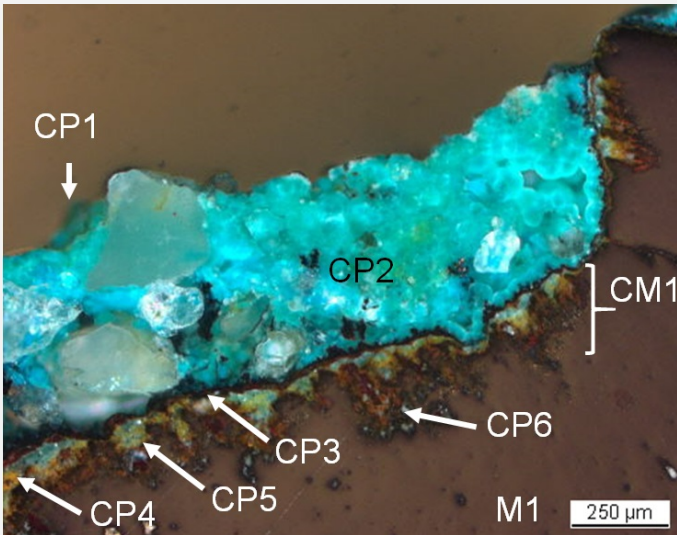
The corrosion crust has a thickness between 0.1mm and 0.7mm (Fig. 8). In bright field (Fig. 11), one can observe that the metal has been replaced by light-grey corrosion products. Adjacent to the metal is a thick, heterogeneous, dark-grey layer with a band of light-grey corrosion products. In polarised light (Fig. 12), all corrosion products which were previously light-grey appear brown-green-yellow, the dark-grey layer being turquoise. The elemental chemical distribution of the SEM images (Figs. 13 and 14) reveals that the inner corrosion products are Sn-rich whereas the adjacent band is Cu and S-rich (Fig. 15). The outer layer contains large inclusions (quartz and others, Si, Al and Na,

see Figs. 14-15) and is most probably composed of malachite/ $\text{Cu}_2(\text{CO}_3)(\text{OH})_2$  (only Cu and O are detected – Fig. 15). S is distributed throughout this layer. XRD analyses indicated the presence of posnjakite/ $\text{Cu}_4\text{SO}_4(\text{OH})_6\text{H}_2\text{O}$ , chalcocite/ $\text{Cu}_2\text{S}$  and djurleite/ $\text{Cu}_{1.93}\text{S}$  (Schweizer 1994).



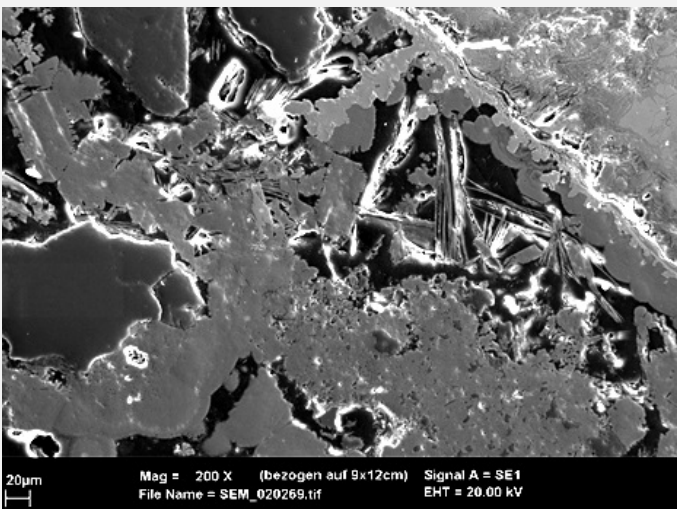
Credit HE-Arc CR.

Fig. 11: Micrograph of the metal sample from Fig. 8 (detail), unetched, bright field. The inner light-grey corrosion products extend into the metal surface (in pink) and appear as a line within the dark-grey corrosion layer,



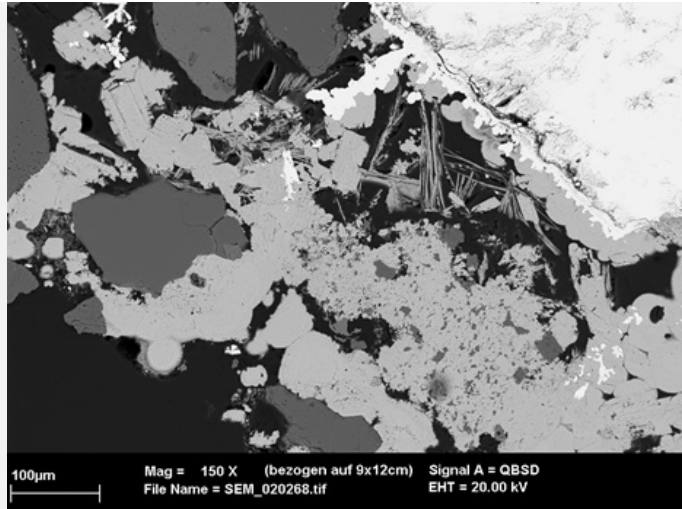
Credit HE-Arc CR.

Fig. 12: Micrograph similar to Fig. 11 and corresponding to the stratigraphy of Fig. 16, polarized light. One can see that large mineral features are incorporated only in the corrosion layers above the brown-orange corrosion band,



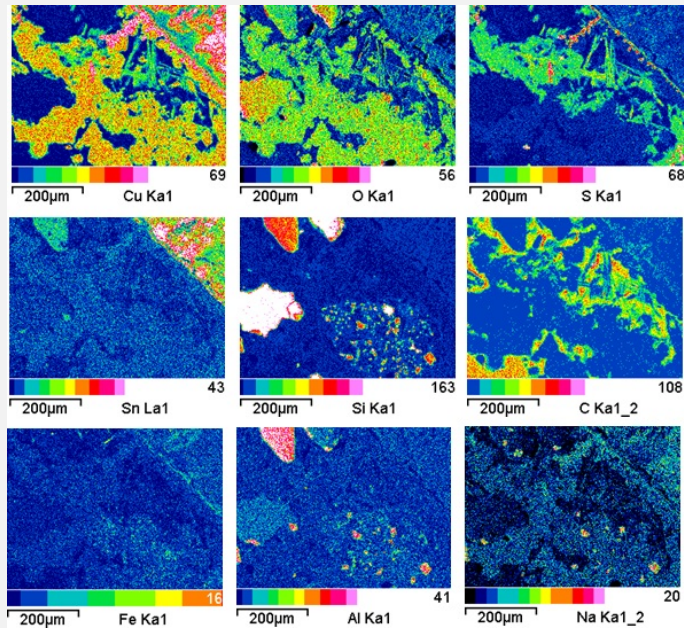
Credit HE-Arc CR.

Fig. 13: SEM image (detail of Fig. 11), SE-mode. From bottom to top right: the thick, porous outer corrosion layer, the light-grey band and the remaining metal,



Credit HE-Arc CR.

Fig. 14: SEM image, similar to Fig. 13, BSE-mode,



Credit Empa.

Fig. 15: EDS elemental chemical distribution of the SEM image of Fig. 13. Method of examination: SEM/EDS, Laboratory of Analytical Chemistry, Empa,

**Corrosion form** Uniform - transgranular

**Corrosion type** Type I (Robbiola)

**Complementary information**

None.

∨ MiCorr stratigraphy(ies) – CS

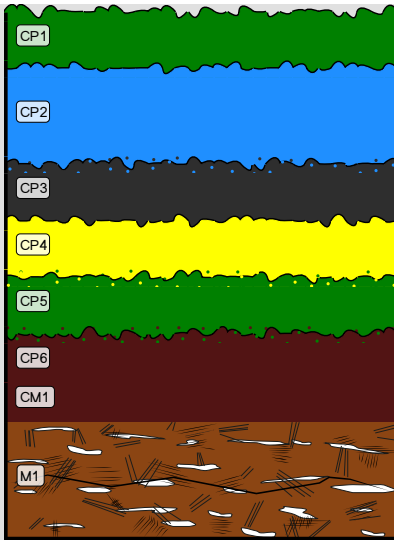


Fig. 16: Stratigraphic representation of the sample taken from the tang fragment in cross-section (dark field) using the MiCorr application. The characteristics of the strata are only accessible by clicking on the drawing that redirects you to the search tool by stratigraphy representation. This representation can be compared to Fig. 12, Credit HE-Arc CR.

### ✓ Synthesis of the binocular / cross-section examination of the corrosion structure

Corrosion products CP2 to CP5 observed under binocular corresponds to CP1 to CP4 under cross-section. The other CPs are more difficult to compare, certainly due to the disruption of the corrosion structure during the cutting process.

### ✓ Conclusion

The tang fragment is made from a bronze and has been cold worked on the top surface after annealing. The past XRD analyses indicate the presence of chalcopryrite in the corrosion crust, typical of lake context (Schweizer 1994), not analysed though with EDX (combinaison of Fe, S and Cu), enriched with Sn close to the metal surface and depleted of Cu on the outer surface. This object was certainly abandoned rather quickly in an anaerobic, humid and S and Fe-rich environment, favouring then the formation of chalcopryrite, before being exposed in an aerated environment in which the crust was formed. The limit of the original surface most probably lies between the Sn-rich inner layer and the Fe and S-rich outer layers. The presence of iron oxides on top of the copper corrosion crust has not yet been explained. The corrosion is a type 1 according Robbiola et al. 1998.

### ✓ References

#### References on object and sample

##### *References object*

1. Rychner-Faraggi A-M. (1993) Hauterive – Champréveyres 9. Métal et parure au Bronze final. Archéologie neuchâteloise, 17 (Neuchâtel).

##### *References sample*

2. Rapport d'examen, Laboratoire Musées d'art et d'histoire, Geneva GE (1987), 87-194 à 197.

3. Schwartz, G.M. (1934) Paragenesis of oxidised ores of copper, Economic Geology, 29, 55-75.

4. Schweizer, F. (1994) Bronze objects from Lake sites: from patina to bibliography. In: Ancient and historic metals, conservation and scientific research (eds. Scott, D.A., Podany, J. and Considine B.B.), The Getty Conservation Institute, 33-50.

#### References on analytic methods and interpretation

5. Robbiola, L., Blengino, J-M., Fiaud, C. (1998) Morphology and mechanisms of formation of natural patinas on archaeological Cu-Sn alloys, *Corrosion Science*, 40, 12, 2083-2111.